

## ENERGY CONVERSION IN SYSTEMS-CONTAINED LASER-IRRADIATED METALLIC NANOPARTICLES – COMPARISON OF RESULTS FROM ANALYTICAL SOLUTIONS AND NUMERICAL METHODS

Piotr RADOMSKI\*, Paweł ZIÓLKOWSKI\*, Dariusz MIKIELEWICZ\*

\* Faculty of Mechanical Engineering and Ship Technology, Institute of Energy,  
Gdańsk University of Technology, Gabriela Narutowicza 11/12, 80-233 Gdańsk, Poland

[piotr.radomski@pg.edu.pl](mailto:piotr.radomski@pg.edu.pl), [pawel.ziolkowski1@pg.edu.pl](mailto:pawel.ziolkowski1@pg.edu.pl), [dariusz.mikielwicz@pg.edu.pl](mailto:dariusz.mikielwicz@pg.edu.pl)

*received 28 February 2023, revised 22 April 2023, accepted 27 April 2023*

**Abstract:** This work introduces the theoretical method of metallic nanoparticles' (NPs') heat and mass transfer where the particles are coated on a surface (base), together with considering the case wherein nanoparticles move freely in a pipe. In order to simulate the heat transfer, energy and radiative transfer equations are adjusted to the considered issue. NPs' properties are determined following the nanofluidic theories, whereas absorption and scattering coefficients are described using either Mie-Lorenz theory or Rayleigh-Drude approximation. Thermal boundary conditions are implemented based on the microscale heat transfer and Smoluchowski theory. Results are compared with the classical Fourier transport differential solutions that have been adjusted to laser irradiation.

**Key words:** energy conversion, heat transfer, metallic nanoparticles, Smoluchowski theory

### 1. INTRODUCTION

Gold nanoparticles (NPs) commonly appeared inside the red-stained glasses in gothic cathedrals during the medieval ages. At that time, however, no one was aware of the dormant potential or the physical reason why these structures possessed a red color instead of a yellowish one. The reason for this phenomenon was discovered by Gustav Mie and Ludvig Lorenz, who proposed around the same time a theoretical explanation for the red-shifted gold properties, stating their theories on the Maxwell equations. Although those works appeared to be perfect for every spherical NP size, there was a problem to describe the interaction for other shapes, e.g. rods, cubes and triangles. However, it has been ascertained that for most shapes, an explicit formulation cannot be determined, and numerical methods should be considered [1–7].

On the other hand, the Rayleigh–Drude approximation is being commonly proposed for calculations of small NPs and gasses, regardless of working environment. As long as this theory is only approximation of the Mie–Lorenz one, and fails under condition  $d \ll \lambda$ , where  $d$  is the nanoparticle diameter, and  $\lambda$  represents the incident wavelength, there are virtually no restrictions on the NP shape, regardless of its complicity.

Both approaches, however, indicate that there exists at least one spectra peak wherein the absorption cross section is maximized. The maximum is searched at the local surface plasmon resonance phenomenon (LSPR) which treats each NP as a set of vibrations – plasmons. If the vibrations' frequency is near the incident wavelength, NPs produce a collective single vibration that, in the absence of electrical or magnetic outlet, is capable only converting of the whole absorbed energy into heat. This potential was generally discerned generally a dozen years ago in

inactivation bioprocesses, e.g. hyperthermia tumors, where temperature increases locally, which minimizes the process invasiveness.

Nevertheless, there is still a lack of theoretical models that may be utilized for such nanomaterials' irradiation. Some of them require complex models that are usually based on DPM models, as has been discussed in [8–11]. This paper considers NPs as a heat source of converted energy. In the literature, such a case was proposed for thin films in the study of Bohren et al. [2,6,12], and now the model has been being developed scrupulously by authors in [13–15] for particles irradiation. The present research also highlights that the irradiation process may be automated in specific cases. Fig. 1. outlines the heat generation processes, which are responsible for the temperature increase, and which may be divided into two general parts – electromagnetic energy conversion into heat and heat transport into the material from NPs' location. Therefore, the control input parameter here is the laser power that establishes principally the heat generation rate and provides the temperature increase. Subsequently, the temperature increase due to the heat transfer model in a material can be stated as the output.

Moreover, it has been emphasized that laser ablation in simple cases may be described and analyzed via classical Fourier heat transfer and its adequate differential solutions. Likewise, the considered model enables the determination of heat transfer between solids. Therefore, the main work's purpose is to propose the heat flux model as a response for the applied laser power as a result of electromagnetic energy conversion into heat. Furthermore, the response is compared with the adapted-to-system temperature relationships that describe the unsteady heat transfer between a solid and metallic NPs or thin films.

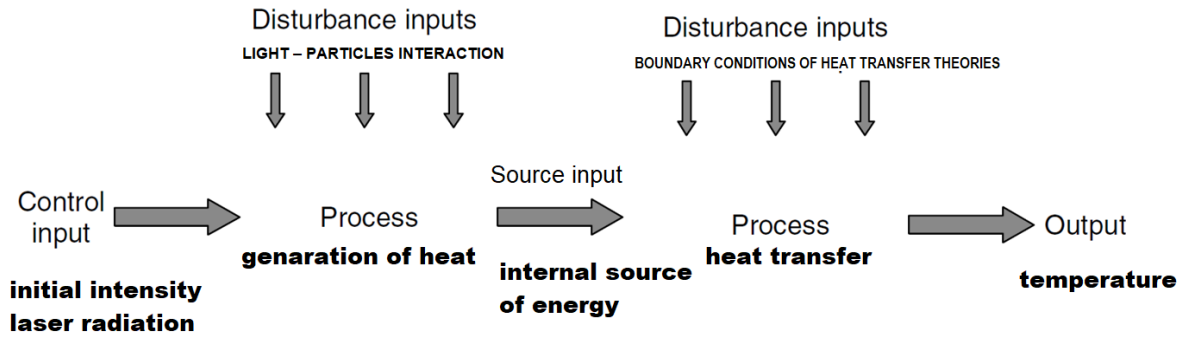


Fig. 1. Process of heat transfer modelling for metallic NPs and thin metallic films

## 2. LIGHT - PARTICLES INTERACTION

### 2.1. Heat transfer equations

Light-matter interaction that includes all classical phenomena is generally described following Eqs. (1) – (4) using the radiative heat transfer approach [12,14,16]:

$$\begin{aligned} & \frac{1}{c} \frac{\partial I_o(r, \Omega, t)}{\partial t} + \text{div} \left( I_o(r, \Omega, t) \cdot \vec{S}(\Omega) \right) + \\ & + \left( \sigma_{\text{abs}_h} + \sigma_{\text{sca}_p} + \sigma_{\text{abs}_p} \right) \cdot I_o(r, \Omega, t) = \\ & = \sigma_{\text{abs}_h} \cdot m_h^2 \cdot \frac{\sigma_{SB} \cdot T^4}{4\pi} + E_p + \\ & + \frac{\sigma_{\text{sca}_p}}{4\pi} \int_0^{4\pi} \left( I_o(r, \Omega, t) \cdot \Phi \left( \vec{S}(\Omega) \right) \right) d\Omega \end{aligned} \quad (1)$$

$$\sigma_{\text{abs}_p} = \xi \cdot \sum_i^N (C_{\text{ext}_i} - C_{\text{sca}_i}) \quad (2)$$

$$\sigma_{\text{sca}_p} = \xi \cdot \sum_i^N (C_{\text{sca}_i}) \quad (3)$$

$$E_p = \xi \cdot \sum_i^N \epsilon_i \cdot A_i \cdot \frac{\sigma_{SB} \cdot T^4}{4\pi} \quad (4)$$

where:  $c$  – speed of light in vacuum ( $\text{m} \cdot \text{s}^{-1}$ ),  $I_o(r, \Omega, t)$  – spatial profile of light incident intensity ( $\text{W} \cdot \text{m}^{-2}$ ),  $t$  – time (s),  $\vec{S}(\Omega)$  – oriented surface ( $\text{m}^2$ ),  $\Omega$  – angle of orientation (rad),  $\sigma_{\text{abs}_h}$  – absorption coefficient of the surrounding medium ( $\text{m}^{-1}$ ),  $\sigma_{\text{sca}_p}$  – scattering coefficient of particles ( $\text{m}^{-1}$ ),  $\sigma_{\text{abs}_p}$  – absorption coefficient of particles ( $\text{m}^{-1}$ ),  $m_h$  – refractive index of the surrounding medium ( - ),  $\sigma_{SB}$  – Stefan-Boltzmann constant ( $\text{W} \cdot \text{m}^{-2} \cdot \text{K}^{-4}$ ),  $T$  – temperature (K),  $E_p$  – emissivity coefficient of particles due to black-body radiation ( $\text{W} \cdot \text{m}^{-3}$ ),  $C_{\text{ext}_i}$  – extinction cross section of the  $i$ -particle ( $\text{m}^2$ ),  $C_{\text{sca}_i}$  – scattered cross section of the  $i$ -particle ( $\text{m}^2$ ),  $\xi$  – nanoparticles concentration ( $\text{m}^{-3}$ ),  $\epsilon_i$  – emissivity of the  $i$ -particle ( - ),  $A_i$  – projected area of the  $i$ -particle ( $\text{m}^2$ ),  $\sum_i^N$  – sum of particle from  $i = 1$  to  $i = N$ .

In case of temperature changes, the energy balance equation would be applied, treating particles as inclusions in fluid or at a solid boundary, basing on the literature, described by Eqs. (5) – (7) [12,14,15,17–19]:

$$\begin{aligned} & \frac{\partial}{\partial t} \left( \alpha_p \cdot \rho \cdot e \right) + \text{div} \left( \alpha_p \cdot \rho \cdot e \vec{v} + \alpha_p \cdot p \vec{v} \right) = \\ & = \text{div} \left( k_{\text{eff}} \cdot \text{grad}(T) + \left( \text{grad}(\overline{X^{\dagger}}) - \mu I_{\vec{d}} \vec{I} + 2\mu \vec{d} \right) \cdot \vec{v} \right) \\ & - g_{e-ph} \cdot (T - T_{ph}) + S^f + S_i^p \\ & + \sum_i \theta_i^{p-f} + \sum_i \theta_i^{p-p} + Q_{in} \end{aligned} \quad (5)$$

$$\begin{aligned} S_i^p & = \sum_i^N \sigma_{\text{abs}_p} \cdot I_{\text{abs}_i} = \xi \cdot \left( 1 - \exp(-\sigma_{\text{abs}_h} \cdot l_f) \right) \cdot \\ & \cdot \left( 1 - \frac{(m_p - m_h)^2 + (\overline{m}_p - \overline{m}_h)^2}{(m_p + m_h)^2 + (\overline{m}_p + \overline{m}_h)^2} \right) \cdot \\ & \cdot \sum_i^N (C_{\text{ext}_i} - C_{\text{sca}_i}) \cdot I_o(r, \Omega, t) \cdot \\ & \cdot \left( 1 - \frac{(m_h - m_a)^2 + \overline{m}_h^2}{(m_h + m_a)^2 + \overline{m}_h^2} \right) \cdot \\ & \cdot \left( 1 - \exp(-\xi \cdot (C_{\text{ext}_i} - C_{\text{sca}_i}) \cdot l_i) \right) \end{aligned} \quad (6)$$

$$\begin{aligned} S^f & = \sigma_{\text{abs}_h} \cdot I_{\text{abs}_h} = \sigma_{\text{abs}_h} \cdot I_o(r, t) \cdot \\ & \cdot \left( 1 - \frac{(m_h - m_a)^2 + \overline{m}_h^2}{(m_h + m_a)^2 + \overline{m}_h^2} \right) \cdot \\ & \cdot \left( 1 - \exp(-\sigma_{\text{abs}_h} \cdot l_f) \right) \end{aligned} \quad (7)$$

where:  $\alpha_p$  – volume of particles' occupation in fluid ( - ),  $\rho$  – density of a material ( $\text{kg} \cdot \text{m}^{-3}$ ),  $e$  – specific energy ( $\text{J} \cdot \text{kg}^{-1}$ ),  $\vec{v}$  – velocity of the fluid ( $\text{m} \cdot \text{s}^{-1}$ ),  $p$  – pressure (Pa),  $k_{\text{eff}}$  – effective thermal conductivity coefficient ( $\text{W} \cdot \text{m}^{-1} \cdot \text{K}^{-1}$ ),  $\overline{X^{\dagger}}$  – diffusive momentum flux ( $\text{kg} \cdot \text{m} \cdot \text{s}^{-2}$ ),  $\mu$  – molecular viscosity ( $\text{kg} \cdot \text{m}^{-1} \cdot \text{s}^{-1}$ ),  $I_{\vec{d}}$  – first invariant of the strain rate ( $\text{s}^{-1}$ ),  $\vec{I}$  – unit tensor ( - ),  $\vec{d}$  – symmetric rate of deformation ( $\text{s}^{-1}$ ),  $g_{e-ph}$  – electron-phonon coupling for nanoparticles ( $\text{W} \cdot \text{m}^{-3} \cdot \text{K}^{-1}$ ),  $T_{ph}$  – temperature of crystal lattice (phonon heat) (K),  $S^f$  – source of energy for fluids ( $\text{W} \cdot \text{m}^{-3}$ ),  $S_i^p$  – source of energy for the  $i$ -particle ( $\text{W} \cdot \text{m}^{-3}$ ),  $\theta_i^{p-f}$  – heat exchange between the  $i$ -particle and fluid ( $\text{W} \cdot \text{m}^{-3}$ ),  $\theta_i^{p-p}$  – heat exchange between particles ( $\text{W} \cdot \text{m}^{-3}$ ),  $Q_{in}$  – internal source of energy, e.g. as a result of the magnetic field presence ( $\text{W} \cdot \text{m}^{-3}$ ),  $I_{\text{abs}_i}$  – absorbed part of the  $i$ -particle ( $\text{W} \cdot \text{m}^{-2}$ ),  $l_f$  – path's length that light passes through fluid (m),  $m_p$  – real part of the refractive index of particle's material ( - ),  $\overline{m}_p$  – imaginary part of the refractive index of particle's material ( - ),  $\overline{m}_h$  – imaginary part of the refractive index of the surrounding medium ( - ),  $m_a$  – refractive index of air ( - ),  $l_i$  – path's length that light passes through the  $i$ -particle (m),  $I_{\text{abs}_h}$  – absorbed part of the surrounding medium ( $\text{W} \cdot \text{m}^{-2}$ ).

Eqs. (6) and (7) were previously examined for metallic thin films [15,17]. In the present study they are adapted to the considered system containing particles. For metallic thin films, specific heat capacity and thermal conductivity are ruled by the heat exchange between electron and crystal lattice interaction regardless of the incident intensity [12,17]. In case of particles as well, this coupling, i.e.  $g_{e-ph}$ , exists as well, however, is much stronger, which reduces the temperature increase [20,21].

Nonetheless, many other problems, pertaining to the NPs' orientation and strain deformation, appear, which cannot be solved accurately. The first one refers to the thermal conductivity that may be treated following many approaches. The most crucial issue here, however, is to include a size and a shape dependence that diminish the thermal conductivity value significantly. For the NP that is of a noble metal, the proceeding may follow Eq. (8) [22–25]:

$$k_{\text{eff},p,i} = \frac{\rho_{p,i} \cdot c_{p,p,i} \cdot \bar{v}_F \cdot \Lambda_o}{3} \cdot \frac{\Lambda_{p,i}}{\Lambda_o} = k_o \cdot \frac{1}{1+Kn} \quad (8)$$

where:  $k_{\text{eff},p,i}$  – thermal conductivity coefficient of the  $i$ -particle ( $W \cdot m^{-1} \cdot K^{-1}$ ),  $\rho_{p,i}$  – density of the  $i$ -particle ( $kg \cdot m^{-3}$ ),  $c_{p,p,i}$  – specific heat capacity of the  $i$ -particle ( $J \cdot kg^{-1} \cdot K^{-1}$ ),  $\bar{v}_F$  – Fermi velocity ( $m \cdot s^{-1}$ ),  $\Lambda_o$  – mean free path of an electron for a bulk metal (m),  $\Lambda_{p,i}$  – mean free path (particle size) of an electron for the  $i$ -particle (m),  $k_o$  – thermal conductivity coefficient of a pure metal ( $W \cdot m^{-1} \cdot K^{-1}$ ), Kn – Knudsen number (-).

Other issues, which are related to the fluid flow, are discussed in the forthcoming subsections.

## 2.2. Cross sections

The most paramount parameters, which are worth a deeper investigation, are NPs' concentration,  $\xi$ , and cross sections. Nanoparticles concentration,  $\xi$ , which is defined as the number of NPs in a selected volume, is not a separated parameter, and indicates the interaction rate between single NPs. Its relationship with cross sections is dependent on the applied theory. This topic was discussed in Gouesbet's study [4,26]. The issue stays the number of nanoparticles concentration at which the interaction starts to be significant, and so far there has been no precise value.

Scattering and extinction cross-section, however, are well-known and may be calculated differently depending on the considered theory. The Mie–Lorenz one presents them as for spheres [2,5,6,12] following Eqs. (9) and (10):

$$C_{\text{ext},i} = \sum_i^N \frac{\lambda^2}{2\pi} \sum_{j=1}^{\infty} (2j+1) \cdot \Re(a_{j,i} + b_{j,i}) \quad (9)$$

$$C_{\text{sca},i} = \sum_i^N \frac{\lambda^2}{2\pi} \sum_{j=1}^{\infty} (2j+1) \cdot (|a_{j,i}|^2 + |b_{j,i}|^2) \quad (10)$$

where:  $\lambda$  – Incident wavelength (m),  $j$  – selected rank of Mie coefficients' accuracy,  $a_{j,i}$  – first Mie coefficient (-),  $b_{j,i}$  – second Mie coefficient (-),  $N$  – number of nanoparticles.

Meanwhile, the Rayleigh–Drude approximation yields Eqs. (11)–(13) [1,6]:

$$C_{\text{ext},i} = 4\pi \cdot \left(\frac{2\pi}{\lambda}\right) \cdot \Im m(\alpha_i) \quad (11)$$

$$C_{\text{sca},i} = \frac{8\pi}{3} \cdot \left(\frac{2\pi}{\lambda}\right)^4 \cdot |\alpha_i|^2 \quad (12)$$

$$\alpha_i = \frac{3V_i}{4\pi} \cdot \frac{(\varepsilon_p + \Im \cdot \tilde{\varepsilon}_p) - (\varepsilon_h + \Im \cdot \tilde{\varepsilon}_h)}{(\varepsilon_p + \Im \cdot \tilde{\varepsilon}_p) + 2 \cdot (\varepsilon_h + \Im \cdot \tilde{\varepsilon}_h)} \quad (13)$$

where:  $\alpha_i$  – polarizability of the  $i$ -particle ( $m^3$ ),  $V_i$  – volume of the  $i$ -particle ( $m^3$ ),  $\varepsilon_p$  – real part of the permittivity of the considered metal (-),  $\tilde{\varepsilon}_p$  – imaginary part of the permittivity of the considered metal (-),  $\varepsilon_h$  – real part of the permittivity of the host medium (-),  $\tilde{\varepsilon}_h$  – Imaginary part of the permittivity of the host medium (-).

It is generally alleged that, for several reasons, the second approach is more amicable compared to the Mie-Lorenz theory. Firstly, the Rayleigh-Drude approximation introduces simple and distinguishable formulas depending on the mean distance between NPs. It has been presented in particular in Bohren and Huffman [6], van de Hulst [2], Siegel and Howell [12] and Voltz [26]. On the other hand, both the Mie-Lorenz and the Rayleigh-Drude approaches may be introduced via the particle's polarizability whose methodology involve to calculate one formula for each shape.

The relationship, however, is usually very tangled for non-spherical particles. Nonetheless, the simplest shapes, spherical and ellipsoidal ones, are well-known for both approaches, and they enable the number of shapes to be expanded with needle (stretched to infinity) and disk (flattened-to-zero thickness) structures at the mathematical limits of a depolarization factor,  $\mathcal{L}_i$ . Then, for the particle oriented along the  $i$ -axis [2,6,12,13], polarizability is presented by Eq. (14):

$$\alpha_{i,i} = \frac{V_i}{4\pi} \cdot \left( \mathcal{L}_i + \left( \frac{(\varepsilon_p + \Im \cdot \tilde{\varepsilon}_p)}{(\varepsilon_h + \Im \cdot \tilde{\varepsilon}_h)} - 1 \right)^{-1} \right)^{-1} \quad (14)$$

For prolate (stretched) structures, Eqs. (15) and (16) are governed:

$$\mathcal{L}_{i,i}^{\text{str}} = \frac{1 - \phi_{i,s}^2}{\phi_{i,s}^2} \cdot \left( \frac{1}{2 \cdot \phi_{i,\text{str}}} \cdot \ln \left( \frac{1 + \phi_{i,\text{str}}}{1 - \phi_{i,\text{str}}} \right) - 1 \right) \quad (15)$$

$$\phi_{i,\text{str}} = \sqrt{1 - \left( \frac{d_{s,i}}{d_{l,i}} \right)^2} \quad (16)$$

whereas for oblate (flattened) ones, Eqs. (17) and (18) yields:

$$\mathcal{L}_{i,i}^{\text{fl}} = \frac{1 + \phi_{i,\text{fl}}^2}{\phi_{i,\text{fl}}^2} \cdot \left( 1 - \frac{1}{\phi_{i,\text{fl}}} \cdot \tan^{-1} \phi_{i,\text{fl}} \right) \quad (17)$$

$$\phi_{i,\text{fl}} = \sqrt{\left( \frac{d_{l,i}}{d_{s,i}} \right)^2 - 1} \quad (18)$$

where:  $d_{l,i}$  – longer diameter of the  $i$ -nanoparticle (m),  $d_{s,i}$  – shorter diameter of the  $i$ -nanoparticle (m).

Some other shapes have been explored using numerical methods, yielding near-accurate results. A 5% approximation was proposed by Kang et al. [27], where it is possible to implement any arbitrary shape, albeit it requires the use of complex hypergeometric mathematical functions. The majority of presented structures are also capable of the “coating” process, which presents an opportunity to investigate another group of hybrid materials or surfactants that are unreacted or attached to a NP's surface compounds. The topic has been detailed in many studies in the literature [2,6,13,28].

## 3. NANOPARTICLES COATED ON A SURFACE

Deposited NPs that are present freely on a surface, or those embedded ones inside a material, seem to be relatively simple, and all nanoparticles may be assumed as stable and non-moving granules at a wall. It should be taken into account, however, that there exist a few issues worth investigating. Firstly, when the prolate or oblate structures are considered, the biggest part of

NPs are oriented in one direction owing to gravity and electrostatic forces. Therefore, the particle's polarizability would be discussed for the one oriented axis.

Another relevant problem is that the LSPR phenomenon implies changing of the light-particle-base interaction. For smooth, polished non-charged materials, such as glasses, it is commonly assumed that the change exists only at the refractive index of the host medium that is defined as (Eq. (19)):

$$m_{h_{sur}} = \frac{m_h + m_{base}}{2} \quad (19)$$

where:  $m_{base}$  – refractive index of the base material on which particles are coated.

If the wall is a charged surface, interaction may be calculated treating NPs and surface as a crib structure at which legs are the NPs and the manger is a base material. Noticeably, the crib becomes a thin film if its thickness is very high and NPs' presence are negligible. Nonetheless, this topic requires sophisticated mathematics and is beyond the considered subject in this work. Some more sophisticated elements have been introduced by Royer et al.[29,30], where the interaction is developed with the NPs' distance.

Furthermore, it has been discovered in the course of research that the heat interaction between particles and fluid,  $\theta_i^{p-f}$ , cannot be treated separately. Among models that perceive the interaction as nanofluids or are based on property's slips, the Smoluchowski model [15,31,32] defines the temperature jump at the body boundaries as a result of conductivity discontinuity. In the case of a fluid containing metallic nanoparticles, this model is extremely major owing to the ranges (for noble metals  $k \sim 400 \text{ W} \cdot \text{m}^{-1} \cdot \text{K}^{-1}$ , for fluids  $k \sim 0.4 \text{ W} \cdot \text{m}^{-1} \cdot \text{K}^{-1}$ ). For particles, the Smoluchowski model follows the energy equation, described by Eq. (20):

$$\begin{aligned} & \frac{\partial}{\partial t} \left( \rho_{p,i} \cdot \left( c_{p,p,i} \cdot T_p + \frac{\vec{v}_{p,i}^2}{2} \right) \right) + \\ & + \text{div} \left( \rho_{p,i} \cdot \left( c_{p,p,i} \cdot T_p + \frac{\vec{v}_{p,i}^2}{2} \right) \cdot \vec{l}_p \cdot \vec{v}_{p,i} \right) + \\ & + \text{div} \left( k_{\text{eff},p,i} \cdot \text{grad}(T_p) \right) + \\ & + l_T^f \cdot (T_S^f - T_S) - l_T^p \cdot (T_S^p - T_S) + \\ & + \alpha_d^f \cdot (T^f - T_S^f) - \alpha_{d,i}^p \cdot (T^p_i - T_S^p) + \\ & + (\vec{q}^f - \vec{q}^p) \cdot \vec{n} + (\vec{F}_m^f \times \vec{v}_{\text{slip}}^f - \vec{F}_m^p \times \vec{v}_{\text{slip}}^p) \cdot \vec{n} \\ & = S^f + S_i^p + Q_{\text{in}} - g_{e-ph} \cdot (T - T_{ph}) \end{aligned} \quad (20)$$

in which:  $T_p$  – temperature of particles (K),  $\vec{v}_{p,i}$  – velocity of the  $i$ -particle ( $\text{m} \cdot \text{s}^{-1}$ ),  $\vec{l}_p$  – idemfactor in reference to particles (-),  $l_T^f$  – discontinuity at the boundary from fluid side,  $T_S^f$  – temperature at the boundary from fluid side (K),  $T_S$  – Smoluchowski temperature jump (K),  $\alpha_d^f$  – thermal diffusivity of the considered fluid ( $\text{m}^2 \cdot \text{s}^{-1}$ ),  $T^f$  – temperature of fluid (K),  $\alpha_{d,i}^p$  – thermal diffusivity of the  $i$ -particle ( $\text{m}^2 \cdot \text{s}^{-1}$ ),  $T^p_i$  – temperature of particles (K),  $T_S^p$  – temperature at the boundary from particle side (K),  $\vec{q}^f$  – Fourier heat flux of fluid ( $\text{W} \cdot \text{m}^{-2}$ ),  $\vec{q}^p$  – Fourier heat flux of the particles ( $\text{W} \cdot \text{m}^{-2}$ ),  $\vec{n}$  – normal vector of the boundary layer (-),  $\vec{F}_m^f$  – mechanical forces of the fluid ( $\text{kg} \cdot \text{m} \cdot \text{s}^{-2}$ ),  $\vec{v}_{\text{slip}}^f$  – velocity slip at fluid boundary ( $\text{m} \cdot \text{s}^{-1}$ ),  $\vec{F}_m^p$  – mechanical forces of the particles ( $\text{kg} \cdot \text{m} \cdot \text{s}^{-2}$ ),  $\vec{v}_{\text{slip}}^p$  – velocity slip at particle boundary ( $\text{m} \cdot \text{s}^{-1}$ ).

The similar approach can be adopted in case of fluids. On the other hand, the Smoluchowski approach seems to be an applicable model in case particles melt locally. The problem, however, occurs at the light-particle interaction. Due to the fact the size and shape decreases, the absorption cross section becomes a function of time, which is not a trivial problem in reference to determination of its form. Moreover, virtually all material properties undergo changes, and the electron-phonon coupling undergoes severe changes.

#### 4. NUMERICAL RESULTS AND HEAT TRANSFER THEORIES

Solving heat differential solutions is not a trivial issue and often requires utilizing numerical methods. Such a situation appears to be applicable to the Smoluchowski theory owing to its complicity. Nevertheless, if only solids are studied, the problem is shortened to the classical Fourier flux systems that have been well-known in the [15,33–35].

The approach is general and offers the solutions for various boundary conditions, and may be adjusted for the irradiated NPs simply. The semi-infinite solid system assumes that the metallic NPs are kept under adiabatic condition ( $\dot{q} = 0$ ), and Eqs. (21) and (22) [34–36] offer:

$$T(x, t) = \sum_i^N I_{\text{abs}_i} \cdot \frac{\sqrt{4 \cdot t \cdot \alpha_d}}{\lambda} \cdot \text{ierfc} \left( \frac{x}{\sqrt{4 \cdot t \cdot \alpha_d}} \right) \quad (21)$$

$$\begin{aligned} \text{ierfc}(\Psi) &= \frac{1}{\sqrt{\pi}} \cdot \exp(-\Psi^2) - \\ &- \Psi \cdot \frac{2}{\pi} \cdot \int_0^\Psi \exp(-\psi^2) d\psi \end{aligned} \quad (22)$$

where:  $x$  – the dimension inside the material (m),  $\alpha_d$  – thermal diffusivity,  $\Psi$  – parameter describing heat flow rate (-),  $\psi$  – selected mathematical variable (-).

Eq. (21), however, should be adjusted for a finite thickness of a material (or distance from a wall),  $\delta$ , in accordance with the specification in Eq. (23):

$$\begin{aligned} T(x, t) &= T_o + \sum_i^N I_{\text{abs}_i} \cdot \frac{\sqrt{4 \cdot t \cdot \alpha_d}}{\lambda} \cdot \\ &\cdot \left( \sum_{\mathbb{k}=0}^{\mathbb{k}_\infty} \left( \text{ierfc} \left( \frac{(2\mathbb{k}+1) \cdot \delta - x}{\sqrt{4 \cdot t \cdot \alpha_d}} \right) \right) + \right. \\ &\left. \sum_{\mathbb{k}=0}^{\mathbb{k}_\infty} \left( \text{ierfc} \left( \frac{(2\mathbb{k}+1) \cdot \delta + x}{\sqrt{4 \cdot t \cdot \alpha_d}} \right) \right) \right) \end{aligned} \quad (23)$$

where:  $\delta$  – thickness of the considered material (m),  $\mathbb{k}$  – selected rank of the heat transfer accuracy,  $\mathbb{k}_\infty$  – rank of the heat transfer, here: 500 (-).

For the perfect case where only one wall is under a heat flux, the formula would be easily simplified to [33,34] Eq. (24):

$$T(x, t) \sim \exp(-\psi \cdot t) \quad (24)$$

For Dirichlet boundary conditions ( $T_w = \text{const}$ ), however, temperature increase changes the relationship, yielding Eq. (25):

$$\begin{aligned} T(x, t) &= T_o + \sum_i^N I_{\text{abs}_i} \cdot \frac{\sqrt{4 \cdot t \cdot \alpha_d}}{\lambda} \cdot \\ &\cdot \left( \sum_{\mathbb{k}=0}^{\mathbb{k}_\infty} (-1)^{\mathbb{k}} \cdot \left( \text{ierfc} \left( \frac{(2\mathbb{k}+1) \cdot \delta - x}{\sqrt{4 \cdot t \cdot \alpha_d}} \right) - \right. \right. \\ &\left. \left. \text{ierfc} \left( \frac{(2\mathbb{k}+1) \cdot \delta + x}{\sqrt{4 \cdot t \cdot \alpha_d}} \right) \right) \right) \end{aligned} \quad (25)$$

where, if every wall is kept under the same outer  $T_w$ , the relationship might be reduced to Eq. (26) [34,36]:

$$T(x, t) \sim \ln(\psi \cdot t) \tag{26}$$

The abovementioned formulas may easily be extended into pulse lasers where heat flux becomes a specified function of time. For metallic NPs, this value refers to the absorbed part of irradiation as long as the NPs do not vary their orientation and are not melted locally [17,34,37]. Although the approach offers a simple relationship and allows estimation of temperature after infinite time, it is dedicated for short-pulse lasers – on the contrary for the continuous ones that do not reach this maximum temperature. It should be emphasized, however, that the comparison appears to correspond to the majority of simple experimental systems.

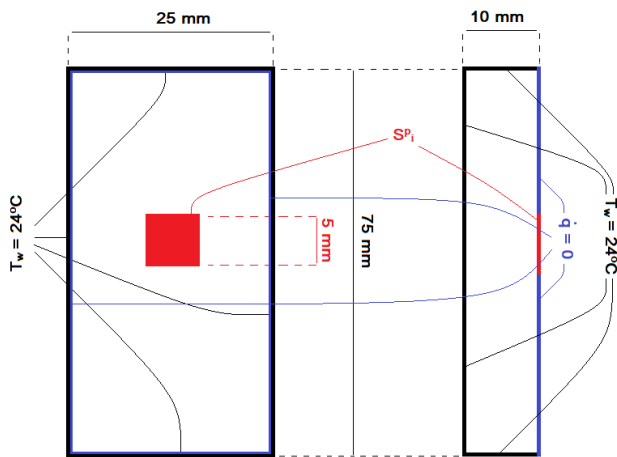


Fig. 2. Scheme of the considered system and applied boundary conditions from [15]

Hence, the temporal results are adopted from the authors' article [15], and demonstrated with the abovementioned temperature relationship due to the fact that the Smoluchowski equation, Eq. (20), is reduced then to the standard energy equation. Fig. 2 repeats the geometry that was utilized in the Radomski et al. [15], whereas Fig. 3 presents the calculated heat generation value (source input). Likewise, Tab. 1, outlines the applied material properties from [15]. Particles, whose diameter is assumed to be 15 nm, are irradiated by a 532-nm laser with the output power 0.8 W. The heat generation rate is calculated analytically using

Tab. 1. Rewritten material parameters from [15] for the theoretical confrontation

Parameter	PDMS	PC	PMMA	Silica glass	Soda-lime glass	Borosilicate glass
Density, $\rho$	965.0	1,198.0	1,184.9	2,200.0	2,464.9	2,124.9
Specific heat capacity, $c_p$	1,460.0	1,199.0	1,456.4	840.0	898.6	779.7
Thermal conductivity, $k$	0.1500	0.2051	0.1912	0.2800	0.1007	1.1489

## 5. NANOPARTICLES IN A PIPE

Free moving NPs incorporated in a fluidic pipe can be treated as a typical phase, e.g. with a mixture or DDPM model regardless of whether the fluid is a gas or liquid. Heat generation may then be ruled based on the Eqs. (6), (7), (9), (20) and (21), and refractive index from Eq. (19) which is governed only near pipe walls

Mie–Lorentz theory. Boundary conditions are supported with the Dirichlet ( $T_w = const$ ) and Neumann approaches using a second-order upwind scheme and the timestep equaled 2 ms. Process of heating was repeated from Fig. 1. Obtained isotherms are highlighted in Figs. 4 whereas output results (points) and the abovementioned relationships (straight curves) are provided in Figs. 5.

The obtained results suggest that the approach corresponds satisfactorily with numerical results. The mismatch might be explained by the complexity of the second approach in the formula and the numerical methods' error.

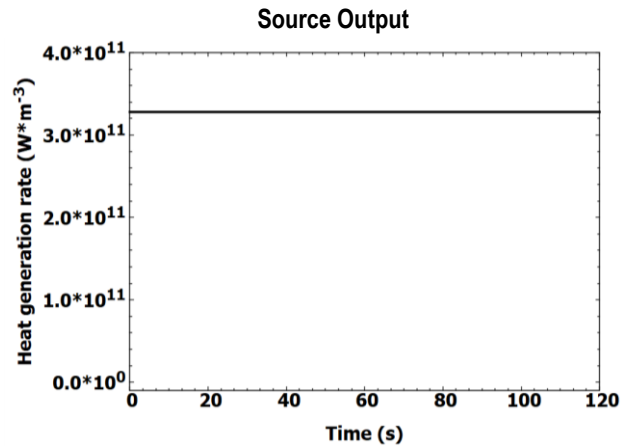


Fig. 3. Time course of the calculated heat generation rate

Considering isotherms, it may be noticed in relation to spherical temperature distributions where  $x$  tends to infinity, which is typical in classical heat transfer solutions, whereas squared shapes appear as a result of heat transfer of gold plate into the isotropic solid. Temperature values depends strongly on thermal diffusivity and heat transfer between gold NPs and the considered base, which indicates that the base's thermal properties should possess lower thermal conductivity in order to maximize temperature, although heat transfer would be more sluggish.

In fluids, however, convection starts to do the lion's share and strongly affects temperature increase. At that situation, temperature relationships become much more tangled to derive and generally numerical methods are indicated to be applied.

and in most cases might be omitted. Likewise, appropriate boundary conditions in reference to microchannels and heat transfer coefficients should be considered. Nevertheless, effective thermal conductivity coefficient,  $k_{eff}$ , should be modeled based on nanofluids for heterogeneous materials. The topic has been considered in the literature that pertains to selected materials [8,12,38–42]. Since particles are not arranged,  $k_{eff}$  follows Eq. (27) [22]:

$$k_{\text{eff}} = k_f \cdot \left( \frac{k_{\text{eff},p,i}}{k_f} \right)^\varphi \quad (27)$$

in which:  $k_f$  – thermal conductivity coefficient of fluid ( $\text{W} \cdot \text{m}^{-1} \cdot \text{K}^{-1}$ ),  $\varphi$  – fraction of occupied particles in fluid (-).

Effective thermal conductivity is realized to be strongly dependent on the occupation fraction of NPs, such as in the Kumar's et al. studies [8,11], and, considering single-phase approach, it may reach even  $10 \text{ W} \cdot \text{m}^{-1} \cdot \text{K}^{-1}$  for  $\varphi = 0.4$ .

In case of forced convection, however,  $\vec{F}_m^f$  and  $\vec{F}_m^p$  are governed by drag forces and they are responsible for particles' rotation. For spherical NPs, the drag coefficient was described by Dennis et al. [43], and Morsi et al. [44], and is governed by Stokes–Cunningham drag law, whereas for non-spherical struc-

tures the topic was discussed in particular by Haider and Levenspiel [45].

However, heat generation becomes much more difficult to estimate for non-spherical particles that are characterized by the full symmetry. For prolate/oblate structures as long as particles are attached to the ground, Eq. (15) or (17) is preserved. At the critical point when particles start to be swept away from the base material, the particles' polarizability ceases to be oriented, changing light–particle interaction into the randomly distributed particles, governed by Eq. (28):

$$\alpha_i = \frac{\alpha_{i,\hat{i}} + \alpha_{i,\hat{j}} + \alpha_{i,\hat{k}}}{3} \quad (28)$$

where:  $\hat{i}, \hat{j}, \hat{k}$  – rectangular coordinates' axes, and  $\hat{i}$  is the oriented one.

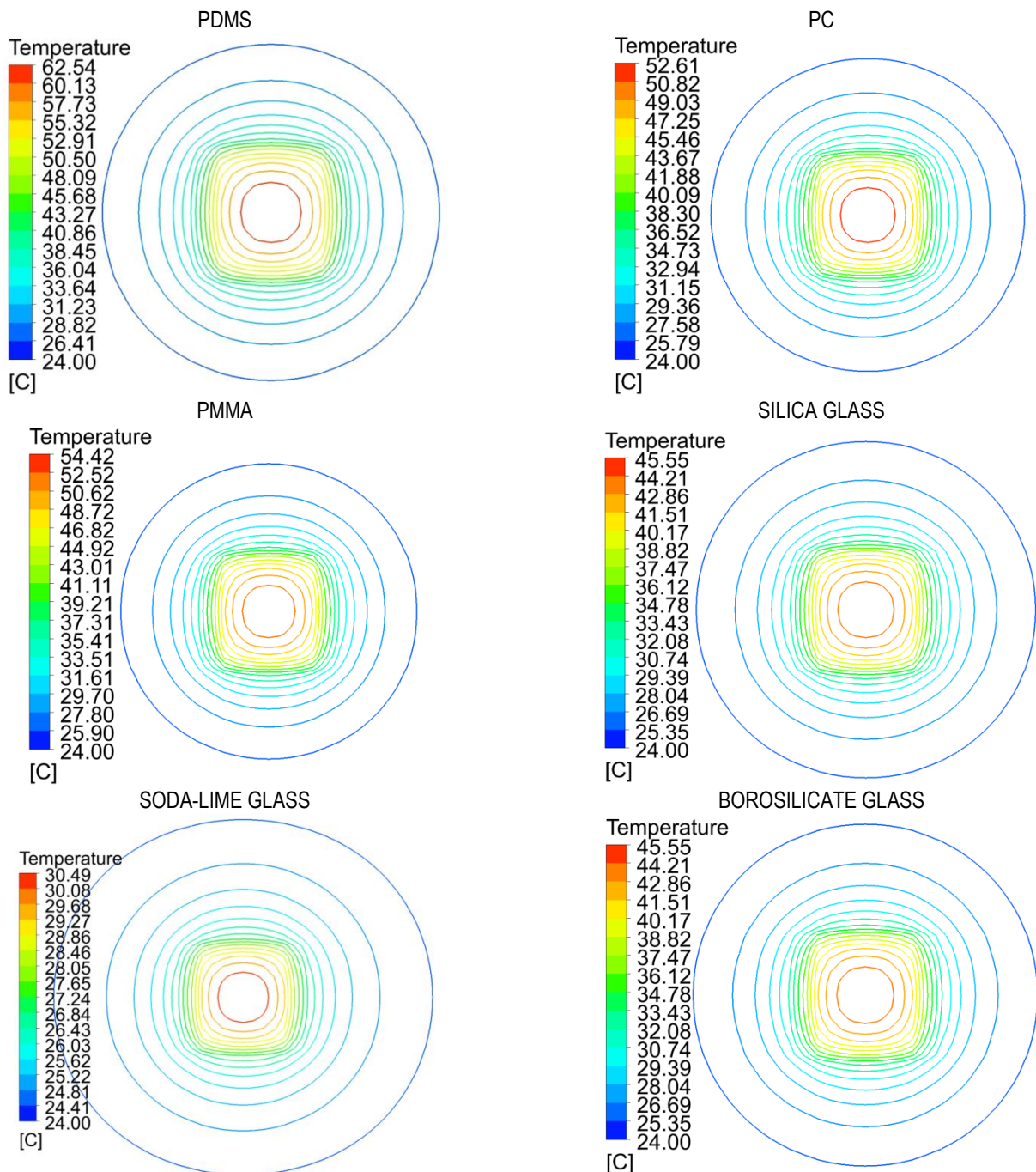


Fig. 4. Isotherms of laser-irradiated materials after 120 seconds using numerical results from [15]

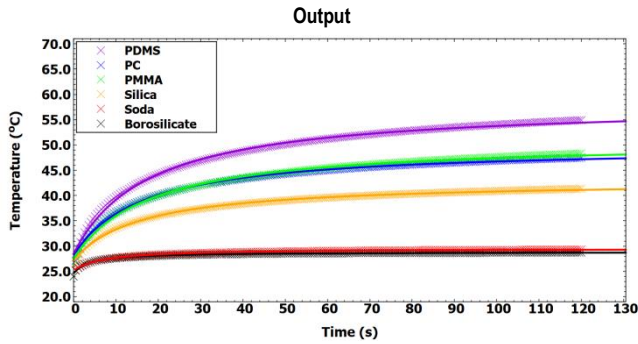


Fig. 5. Temperature time response for the utilized heat generation rate using numerical results (color points) from [15] and the (23)-and-(25)-based relationship (straight curves)

Eq. (15) or (17) is continued if particles stop rotating and every streamline is parallel along the great diameter, which occurs at high speed flows and at a high Reynolds number, however, shear stresses do the lion's share and it should be assumed that they do not affect the particle's shape during its movement.

The problem disappears while the NPs are substituted with a continuous thin film. Although its discretization requires to omit many multiscale issues, treating the material as a slab this problem can be reduced, and only appropriately determination of the heat transfer coefficient and the heat flux rate is needed.

Moreover, for high speed flows, particles are exposed to high shear stresses. This situation is much further complicated if a pipe is highly curved. In that case, NPs' heat generation rate should be governed by the full Mie theory including particle orientation [6,46]. Shear stresses may be modeled based on condensation phenomena between liquid and solid or liquid and gas [47,48]. Nevertheless, a Smoluchowski temperature jump might still be applied, investigating microscale heat transfer between fluid and particles.

## 6. SUMMARY

The present research involves conducting an investigation of ascertaining which parameters are crucial to the simulation of heat transfer of the radiated particles, and discovering that it is a complex issue. On the one hand, both interactions between particles and fluid and particles themselves should be considered, which is also not trivial. For instance, heat generation rate is dependent on many different factors that become highly tangled. Nevertheless, the Rayleigh-Drude approximation provides concisely the particles-particles interaction that may be modeled and implemented easily. However, there is a conflict with regard to the NP's size between the Mie-Lorenz theory, which is only relatively simple for spheres, and the Rayleigh-Drude approximation, which enables modeling any NP's shapes, although it fails when NP's diameter is similar to the incident wavelength. Mie theory is suggested to support the spherical and coated spheres, whereas for more complicated shapes the Rayleigh-Drude approximation can be preferred.

Moreover, fluid-particles interaction is still being studied at present and there is no one, general theory that may be performed to describe heat transport due to different material phenomena. Nonetheless, Smoluchowski theory is highly recommended for any particles-contained system due to its versatile legitimacy, starting from a high difference of thermal conductivity

between particles and fluids and extending up to fluid-particles interaction, which includes boundary phenomena, velocity slips and materials melting. This theory is subjected to the considered system, providing the results' accuracy and a scientific framework under which both the theory and the model would be studied.

## NOMENCLATURE

### Roman letters:

$A_i$	-	Projected area of the $i$ -particle ( $m^2$ )
$a_{j,i}$	-	First Mie coefficient (-)
$b_{j,i}$	-	Second Mie coefficient (-)
$C_{ext,i}$	-	Extinction cross section of the $i$ -particle ( $m^2$ )
$C_{p,p,i}$	-	Heat capacity of the $i$ -particle ( $J \cdot K^{-1}$ )
$C_{sca,i}$	-	Scattered cross section of the $i$ -particle ( $m^2$ )
$c$	-	Speed of light in vacuum ( $m \cdot s^{-1}$ )
$c_p$	-	Specific heat capacity of a material ( $J \cdot kg^{-1} \cdot K^{-1}$ )
$c_{p,p,i}$	-	Specific heat capacity of the $i$ -particle ( $J \cdot kg^{-1} \cdot K^{-1}$ )
$\vec{d}$	-	Symmetric rate of deformation ( $s^{-1}$ )
$d_{l,i}$	-	Longer diameter of the $i$ -nanoparticle (m)
$d_{s,i}$	-	Shorter diameter of the $i$ -nanoparticle (m)
$E_p$	-	Emissivity coefficient of the $i$ -particle due to black-body radiation ( $W \cdot m^{-3}$ )
$e$	-	Specific energy ( $J \cdot kg^{-1}$ )
$\vec{F}_m^f$	-	Mechanical forces of the fluid ( $kg \cdot m \cdot s^{-2}$ )
$\vec{F}_m^p$	-	Mechanical forces of the particles ( $kg \cdot m \cdot s^{-2}$ )
$g_{e-ph}$	-	Electron-phonon coupling for nanoparticles ( $W \cdot m^{-3} \cdot K^{-1}$ )
$I_o(r, \Omega, t)$	-	Spatial profile of light incident intensity ( $W \cdot m^{-2}$ )
$I_{abs_h}$	-	Absorbed part of the surrounding medium ( $W \cdot m^{-2}$ )
$I_{abs_i}$	-	Absorbed part of the $i$ -particle ( $W \cdot m^{-2}$ )
$I_{\vec{d}}$	-	First invariant of the strain rate ( $s^{-1}$ )
$\vec{I}$	-	Unit tensor (-)
$\vec{I}_p$	-	Idemfactor in reference to particles (-)
$\hat{i}, \hat{j}, \hat{k}$	-	rectangular coordinates' axes
$j$	-	Selected rank of Mie coefficients' accuracy
$Kn$	-	Knudsen number (-)
$k$	-	Selected rank of the heat transfer accuracy
$k$	-	Thermal conductivity coefficient ( $W \cdot m^{-1} \cdot K^{-1}$ )
$k_{\infty}$	-	Rank of the heat transfer, here: 500 (-)
$k_o$	-	Thermal conductivity coefficient of a pure metal ( $W \cdot m^{-1} \cdot K^{-1}$ )
$k_{eff}$	-	Effective thermal conductivity coefficient ( $W \cdot m^{-1} \cdot K^{-1}$ )
$k_f$	-	Thermal conductivity coefficient of fluid ( $W \cdot m^{-1} \cdot K^{-1}$ )
$k_{eff_{p,i}}$	-	Thermal conductivity coefficient of the $i$ -particle ( $W \cdot m^{-1} \cdot K^{-1}$ )
$l_f$	-	Path's length that light passes through fluid (m)
$l_i$	-	Path's length that light passes through the $i$ -particle (m)
$l_T^f$	-	Discontinuity at the boundary from fluid side (m)
$l_T^p$	-	Discontinuity at the boundary from particle side (m)
$m_a$	-	Refractive index of air (-)
$m_h$	-	Real part of refractive index of the surrounding medium (-)
$m_p$	-	Real part of the refractive index of particle's material (-)
$\tilde{m}_h$	-	Imaginary part of the refractive index of the surrounding medium (-)

$\widetilde{m}_p$	- Imaginary part of the refractive index of particle's material (-)
$\vec{n}$	- Normal vector of the boundary layer (-)
$p$	- Pressure (Pa)
$Q_{in}$	- Internal source of energy, e.g. as a result of the magnetic field presence ( $W \cdot m^{-3}$ )
$\vec{q}^f$	- Fourier heat flux of fluid ( $W \cdot m^{-2}$ )
$\vec{q}^p$	- Fourier heat flux of particles ( $W \cdot m^{-2}$ )
$r$	- Radius – spherical coordinate (m)
$S^f$	- Source of energy for fluids ( $W \cdot m^{-3}$ )
$S_i^p$	- Source of energy for the $i$ -particle ( $W \cdot m^{-3}$ )
$\vec{S}$	- Oriented surface ( $m^2$ )
$T$	- Temperature (K)
$T^f$	- Temperature of fluid (K)
$T^p_i$	- Temperature of particles (K)
$T_o$	- Initial temperature at the $t = 0$ s (K)
$T_{ph}$	- Temperature of crystal lattice (phonon heat) (K)
$T_S$	- Smoluchowski temperature jump (K)
$T_S^f$	- Temperature at the boundary from fluid side (K)
$T_S^p$	- Temperature at the boundary from particle side (K)
$T_w$	- Wall temperature (K)
$t$	- Time (s)
$V_i$	- Volume of the $i$ -particle ( $m^3$ )
$\vec{v}_F$	- Fermi velocity ( $m \cdot s^{-1}$ )
$\vec{v}$	- Velocity of the fluid ( $m \cdot s^{-1}$ )
$\vec{v}_{p,i}$	- Velocity of the $i$ -particle ( $m \cdot s^{-1}$ )
$\vec{v}_{slip}^f$	- Velocity slip at fluid boundary ( $m \cdot s^{-1}$ )
$\vec{v}_{slip}^p$	- Velocity slip at particle boundary ( $m \cdot s^{-1}$ )
$\vec{X}^\dagger$	- Diffusive momentum flux ( $kg \cdot m \cdot s^{-2}$ )
$x$	- Selected dimension (m)

#### Greek letters:

$\alpha_i$	- Polarizability of the $i$ -particle ( $m^3$ )
$\alpha_p$	- Volume of particles' occupation in fluid (-)
$\alpha_d$	- Thermal diffusivity ( $m^2 \cdot s^{-1}$ )
$\alpha_d^f$	- Thermal diffusivity of the considered fluid ( $m^2 \cdot s^{-1}$ )
$\alpha_{d,i}^p$	- Thermal diffusivity of the $i$ -particle ( $m^2 \cdot s^{-1}$ )
$\delta$	- Thickness of the considered material (m)
$\epsilon_h$	- Real part of the permittivity of the host medium (-)
$\epsilon_p$	- Real part of the permittivity of the considered metal (-)
$\widetilde{\epsilon}_h$	- Imaginary part of the permittivity of the host medium (-)
$\widetilde{\epsilon}_p$	- Imaginary part of the permittivity of the considered metal (-)
$\epsilon_i$	- Emissivity of the $i$ -particle (-)
$\theta_i^{p-f}$	- Heat exchange between the $i$ -particle and fluid ( $W \cdot m^{-3}$ )
$\theta_i^{p-p}$	- Heat exchange between particles ( $W \cdot m^{-3}$ )
$\Lambda_o$	- Mean free path of an electron for a bulk metal (m)
$\Lambda_{p,i}$	- Mean free path (particle size) of an electron for the $i$ -particle (m)
$\lambda$	- Incident wavelength (m)
$\mu$	- Molecular viscosity ( $kg \cdot m^{-1} \cdot s^{-1}$ )
$\xi$	- Nanoparticles concentration ( $m^{-3}$ )
$\rho$	- Density of a material ( $kg \cdot m^{-3}$ )
$\rho_{p,i}$	- Density of the $i$ -particle ( $kg \cdot m^{-3}$ )
$\sigma_{SB}$	- Stefan-Boltzmann constant ( $W \cdot m^{-2} \cdot K^{-4}$ )
$\sigma_{abs_h}$	- Absorption coefficient of the surrounding medium ( $m^{-1}$ )
$\sigma_{abs_p}$	- Absorption coefficient of particles ( $m^{-1}$ )
$\sigma_{sca_p}$	- Scattering coefficient of particles ( $m^{-1}$ )
$\varphi$	- Fraction of occupied particles in fluid (-)

$\Phi$	- Oriented surface
$\phi_{i,fl}$	- Parameter describing aspect ratio of the flattened $i$ -particle (-)
$\phi_{i,str}$	- Parameter describing aspect ratio of the stretched $i$ -particle (-)
$\Psi$	- Parameter describing heat flow rate (-)
$\psi$	- Selected mathematical variable (-)
$\Omega$	- Angle of orientation (rad)

#### Others:

$\partial$	- Symbol of partial derivative
$\Pi_i$	- Depolarization factor of the $i$ -nanoparticle (-)
$\Pi_i^{fl}$	- Depolarization factor of the flattened $i$ -nanostructure (-)
$\Pi_i^{str}$	- Depolarization factor of the stretched $i$ -nanostructure (-)
$\mathbb{I}$	- Symbol of imaginary unit
$\text{imm}$	- Imaginary part of a complex expression
$\text{re}$	- Real part of a complex expression

#### Subscripts and superscripts:

'	- Symbol of derivative
.	- Symbol of scalar product
$\times$	- Symbol of vector product
$a$	- Air
$d$	- Diffusivity
$e^-$	- Electron
$F$	- In reference to Fermi (crystallography)
$f$	- Fluid
$i$	- Selected number
$m$	- Mechanical
$N$	- Number of nanoparticles
$o$	- In reference to initial conditions
$p$	- Particle
$\dagger$	- Transposition

#### Abbreviations:

<i>abs</i>	- Absorption
<i>base</i>	- Base – a material on which nanoparticles are coated
<i>div</i>	- Divergence
<i>eff</i>	- Effective
<i>exp</i>	- Exponent
<i>ext</i>	- Extinction
<i>fl</i>	- Flattened
<i>grad</i>	- Gradient
<i>ierfc</i>	- Short form for error-based functions
<i>in</i>	- Internal
<i>ln</i>	- Symbol of natural logarithm
<i>NPs</i>	- Nanoparticles
<i>ph</i>	- Phonon
<i>SB</i>	- Stefan-Boltzmann
<i>sca</i>	- Scattering
<i>slip</i>	- Slip at the boundary
<i>str</i>	- Stretched
<i>sur</i>	- Surface

#### REFERENCES

1. Strutt JW. On the scattering of light by small particles. London, Edinburgh, Dublin Philos Mag J Sci. 1871;41(275):447–54.
2. van de Hulst HC. Light scattering by small particles. Dover Publications, Inc. New York: John Wiley & Sons; 1957.
3. Lorenz L. Light propagation in and outside a sphere illuminated by plane waves of light. Eur Phys J H. 2019;44(2):77–135.




4. Gouesbet G. Generalized Lorenz-Mie theories and mechanical effects of laser light, on the occasion of Arthur Ashkin's receipt of the 2018 Nobel prize in physics for his pioneering work in optical levitation and manipulation: A review. *J Quant Spectrosc Radiat Transf.* 2019;225:258–77.
5. Mie G. Beiträge zur Optik trüber Medien, speziell kolloidaler Metallösungen. *Ann Phys.* 1908;25(3):377–445.
6. Bohren CF. Absorption and scattering of light by small particles. Absorption and scattering of light by small particles. 1983.
7. Martin RJ. Mie scattering formulae for non-spherical particles. *J Mod Opt.* 1993;40(12):2467–94.
8. Kumar S, Prasad SK, Banerjee J. Analysis of flow and thermal field in nanofluid using a single phase thermal dispersion model. *Appl Math Model* [Internet]. 2010;34(3):573–92. Available from: <http://dx.doi.org/10.1016/j.apm.2009.06.026>
9. Hussain SM, Goud BS, Madheshwaran P, Jamshed W, Pasha AA, Safdar R, et al. Effectiveness of Nonuniform Heat Generation (Sink) and Thermal Characterization of a Carreau Fluid Flowing across a Nonlinear Elongating Cylinder: A Numerical Study. *ACS Omega.* 2022;7(29):25309–20.
10. Hussain SM, Jamshed W, Pasha AA, Adil M, Akram M. Galerkin finite element solution for electromagnetic radiative impact on viscous Williamson two-phase nanofluid flow via extendable surface. *Int Commun Heat Mass Transf* [Internet]. 2022;137:106243. Available from: <https://doi.org/10.1016/j.icheatmasstransfer.2022.106243>
11. Shamsuddin MD, Abderrahmane A, Koullali A, Eid MR, Shahzad F, Jamshed W. Thermal and solutal performance of Cu/CuO nanoparticles on a non-linear radially stretching surface with heat source/sink and varying chemical reaction effects. *Int Commun Heat Mass Transf* [Internet]. 2021;129:105710. Available from: <https://doi.org/10.1016/j.icheatmasstransfer.2021.105710>
12. Siegel R, Howell JR. Thermal radiation heat transfer - Third Edition. Hemisphere Publishing Corporation. 1992.
13. Zaccagnini F, Radomski P, Sforza ML, Ziółkowski P, Lim S-I, Jeong K-U, et al. White light thermoplasmonic activated gold nanorod arrays enable the photo-thermal disinfection of medical tools from bacterial contamination. *J Mater Chem B.* 2023;
14. Radomski P, Ziółkowski P, De Sio L, Mikielawicz D. Importance and form of source element in the energy equation in reference to the photothermoablation of thin films and nanoparticles. In: 9th Wdzydzeanum Workshop on Fluid-Solid Interaction. 2021. p. 24.
15. Radomski P, De Sio L, Mikielawicz D. Computational fluid dynamics simulation of heat transfer from densely packed gold nanoparticles to isotropic media. *Arch Thermodyn.* 2021;42(3):87–113.
16. Michaelides EE. Transport properties of nanofluids. A critical review. Vol. 38, *Journal of Non-Equilibrium Thermodynamics.* 2013. 1–79 p.
17. E. Black S. Laser Ablation: Effects and Applications. New York; 2011. 99–226 p.
18. Ziółkowski P, Szewczuk-Krypa N, Butterweck A, Stajinke M, Gluch S, Drosińska-Komor M, et al. Comprehensive thermodynamic analysis of steam storage in a steam cycle in a different regime of work: A zero-dimensional and three-dimensional approach. *J Energy Resour Technol.* 1899;143(5):050905.
19. Mochnecki B, Paruch M. Cattaneo-Vernotte bio-heat transfer equation. Identification of external heat flux and relaxation time in domain of heated skin tissue. *Comput Assist Methods Eng Sci.* 2018;25(2–3):71–80.
20. Zheng Q, Shen X, Sokolowski-Tinten K, Li RK, Chen Z, Mo MZ, et al. Dynamics of Electron-Phonon Coupling in Bicontinuous Nanoporous Gold. *J Phys Chem C.* 2018;122(28):16368–73.
21. Medvedev N, Milov I. Electron-Phonon Coupling and Nonthermal Effects in Gold Nano-Objects at High Electronic Temperatures. *Materials (Basel).* 2022;15(14):1–11.
22. Warriar P, Teja A. Effect of particle size on the thermal conductivity of nanofluids containing metallic nanoparticles. *Nanoscale Res Lett.* 2011;6(1):247.
23. Feng B, Li Z, Zhang X. Prediction of size effect on thermal conductivity of nanoscale metallic films. *Thin Solid Films.* 2009;517(8):2803–7.
24. Wang BX, Zhou LP, Peng XF. Surface and size effects on the specific heat capacity of nanoparticles. *Int J Thermophys.* 2006;27(1):139–51.
25. Smoluchowski M. O przewodnictwie cieplnem gazów według dotychczasowych teoryj i doświadczeń. *Pr Mat.* 1898;10(12):33–64.
26. Sebastian V, Carminat R, Chantrenne P, Dilhaire S. Microscale and Nanoscale Heat Transfer. Vol. 9, *Optics & Laser Technology.* Berlin; 2007.
27. Kang Y, Zhao Z, Li B. A method for calculating average electric polarizability density of arbitrary small aperture. *J Phys Conf Ser.* 2018;1074(1).
28. Sihvola A, Lindell I V. Polarizability and effective permittivity of layered and continuously inhomogeneous dielectric ellipsoids. *J Electromagn Waves Appl.* 1990;4(1):1–26.
29. Royer P, Bijeon JL, Goudonnet JP, Inagaki T, Arakawa ET. Optical absorbance of silver oblate particles. Substrate and shape effects. *Surf Sci.* 1989;217(1–2):384–402.
30. Royer P, Goudonnet JP, Warmack RJ, Ferrell TL. Substrate effects on surface-plasmon spectra in metal-island films. *Phys Rev B.* 1987;35(8):3753–9.
31. Smoluchowski M. On conduction of heat by rarefied gases. Vol. 46, *The London, Edinburgh, and Dublin Philosophical Magazine and Journal of Science.* 1898. p. 192–206.
32. Smoluchowski M V. Über den Temperatursprung bei Wärmeleitung in Gasen. Vol. 108, *Akademie der Wissenschaften, Wien.* 1898. p. 304–329.
33. Adamowicz A. Determination of Thermal Diffusivity Values Based on the Inverse Problem of Heat Conduction - Numerical Analysis. *Acta Mech Autom.* 2022;16(4):399–407.
34. Carslaw HS, Jaeger JC. Conduction of Heat in Solids. Oxford University Press. London; 1959.
35. Domański R. Promieniowanie laserowe - oddziaływania na ciała stałe. Wydawnictwa Naukowo-Techniczne. Warszawa; 1990. 85–220 p.
36. Ready JF. Mechanism of electron emission produced by a giant-pulse laser. *Phys Rev.* 1965;137(2A):A620–3.
37. Bhandari A. Mathematical Modelling of Water-Based Fe<sub>3</sub>O<sub>4</sub>Nanofluid Due to Rotating Disc and Comparison with Similarity Solution. *Acta Mech Autom.* 2021;15(3):113–21.
38. Kumar R, Singh G, Mikielawicz D. A New Approach for the Mitigating of Flow Maldistribution in Parallel Microchannel Heat Sink. *J Heat Transfer.* 2018;140(7).
39. Szymanski P, Mikielawicz D. Additive Manufacturing as a Solution to Challenges Associated with Heat Pipe Production. *Materials (Basel).* 2022;15(4).
40. Blauciak K, Szymanski P, Mikielawicz D. The influence of loop heat pipe evaporator porous structure parameters and charge on its effectiveness for ethanol and water as working fluids. *Materials (Basel).* 2021;14(22).
41. Miri R, Abbassi MA, Ferhi M, Djebali R. Second Law Analysis of MHD Forced Convective Nanoliquid Flow Through a Two-Dimensional Channel. *Acta Mech Autom.* 2022;16(4):417–31.
42. Hafeez MB, Krawczuk M, Shahzad H. An Overview of Heat Transfer Enhancement Based Upon Nanoparticles Influenced By Induced Magnetic Field with Slip Condition Via Finite Element Strategy. *Acta Mech Autom.* 2022;16(3):200–6.
43. Dennis SCR, Singh SN, Ingham DB. The steady flow due to a rotating sphere at low and moderate Reynolds numbers. *J Fluid Mech.* 1980;101(2):257–79.
44. Morsi SA, Alexander AJ. An investigation of particle trajectories in two-phase flow systems. *J Fluid Mech.* 1972;55(2):193–208.
45. Levenspiel O., Haider A. Drag Coefficient and Terminal Velocity of Spherical and Nonspherical Particles. *Powder Technol.* 1989;58:63–70.
46. Yang P, Wendisch M, Bi L, Kattawar G, Mishchenko M, Hu Y. Dependence of extinction cross-section on incident polarization state and particle orientation. *J Quant Spectrosc Radiat Transf.* 2011;112(12):2035–9.

47. Mikielewicz D. Hydrodynamics and heat transfer in bubbly flow in the turbulent boundary layer. *Int J Heat Mass Transf.* 2003;46(2):207–20.
48. Mikielewicz D, Wajs J, Andrzejczyk R, Klugmann M. Pressure drop of HFE7000 and HFE7100 during flow condensation in minichannels. *Int J Refrig* [Internet]. 2016;68:226–41. Available from: <http://dx.doi.org/10.1016/j.ijrefrig.2016.03.005>

**Acknowledgements:** This research was funded in whole by National Science Centre in Poland under the project „Shape and displacement optimization of gold nanorods in the killing chamber in order to photothermoablation process-es”, no UMO-2021/43/D/ST8/02504. For the purpose of Open Access, the author has applied a CC-BY public copyright licence to any Author Accepted Manuscript (AAM) version arising from this submission.

Computations were carried out using the computers of Centre of Informatics Tricity Academic Supercomputer & Network (CI TASK).

Piotr Radomski:  <https://orcid.org/0000-0002-4778-8670>

Pawel Ziolkowski:  <https://orcid.org/0000-0001-7480-0420>

Dariusz Mikielewicz:  <https://orcid.org/0000-0001-8267-7194>



This work is licensed under the Creative Commons BY-NC-ND 4.0 license.